Materials Science Forum Vol. 232 (1996) pp. 275-294

Inorganic Fullerenes from 2-D Layered Compounds

R. Tenne

Department of Materials and Interfaces, Weizmann Institute, Rehovot 76100, Israel

Keywords: Fullerenes, Inorganic Fullerenes, Layered Compounds, Nanotubes

Abstract

Graphite is the most stable form of carbon at ambient conditions. However, if nanoscopic clusters of graphite are formed they are unstable against bending and closure, due to the large surface energy associated with the dangling bonds of the atoms in the periphery of the clusters. Closed hollow structures designated *fullerenes* are formed, which is considered to be a new form of carbon.

Using the paradigm or carbon fullerenes, it is shown that nanoparticles of inorganic compounds with a layered structure, like MoS_2, are unstable against bending, and form hollow closed clusters, designated *inorganic fullerenes* (IF). The analogy can be extended to similar nanostructures, like nanotubes (NT), nested fullerenes, fullerenes with negative curvature, etc. Various synthetic routes are used to obtain isolated phases of IF. Depending on the structure of the unit cell of the layered compound, apexes of a different topology, like triangles, rectangles, and octagons can be invoked, as well as pentagons and heptagons which are found to be stable elements in carbon fullerenes. Experimental and theoretical considerations are used to elucidate the structure of IF.

1. Introduction

1.1 Structure of nanocrystalline materials

The idea that nanocrystalline phases of a given material may adopt a radically different lattice structure from the bulk solid, is not new. The mathematical basis for this kind of transformation was developed in the early sixties [1]. Based on evidence from X-ray diffraction, it was concluded that amorphous metals (and metal alloys) consist of icosahedral clusters which have distinctly different structure from the face center cubic (fcc) lattice of the bulk material [2-4]. Supercooling of liquid metals was attributed to the prevalence of a 13 atom icosahedral clusters near the freezing point [5]. These clusters are responsible for the delay in the crystallization of the bulk fcc material. Analogous transformations of certain metal alloys into amorphous phase consisting of icosahedral nanoclusters, occur under pressure [6].

Nanocrystals of sizable dimensions (up to ca.10nm), in which each atom preserves its distorted sp^3 structure, but a superstructure of multiply twinned dodecahedral or icosahedral symmetry [7-10] were observed, using transmission electron microscopy (TEM) for some metals (Au, Ag, Ni, Mg) and crystallites of rare gasses, like Ar [11], obtained at low temperatures. The small lattice distortion (5%) caused by such rearrangements leads to an elastic strain which is more than compensated by the large gain in cohesive energy of the cluster, due to the larger average coordination number of the atoms. For larger crystallites a macroscopic gap opens between the twins of the crystallites, which render them unstable. Thus, for macroscopic crystallites the fcc structure is preferred [10]. Theoretical calculations have indicated that metallic clusters, smaller than 2000 atoms, are most stable in the icosahedral structure [12,13]. Above this size a range of intermediate structures where proposed. The same theory has shown that the fcc lattice is stable for crystallites larger than ca. 20,000 atoms. The phase change of a nanoparticle, e.g. icosahedral to cubooctahedral transformation, was found to be non-diffusive in nature, i.e. small rearrangements of the atoms is sufficient to transform the lattice from one structure to another. In other cases however (Pd, Pt, Cu) the nanoparticles were found to adopt the same structure as the bulk solid (fcc) [14].

It is more difficult to envision structural changes of such a magnitude in covalent (or ionic) solids, where hybridization of the orbitals force the nearest neighbors to arrange in a precise angle, with respect to each other. Even small deviations from such angles are energy costly and hence prohibitive, in general. Structural models for amorphous semiconductors like Si, in which packing of 13, 33 or more atoms in icosahedral clusters, were nevertheless proposed [15,16]. To avoid the lattice relaxation necessary for the space feeling, either dislocations of various kinds or hydrogen atoms adsorbed to the dangling bonds were postulated. Iijima [17] found that Si tends to form multiply twinned nanocrystallites of 5-fold symmetry as well. Nonetheless, bond angle and distance in the new nanocrystalline structure of Si atoms, are almost unaltered compared with the diamond lattice. Structural changes of nanocrystallites and colloids of semiconductors with tetrahedral bonding (CdSe), or octahedral hybridization (TiO_2), to e.g. rack-salt structure, were found, under large pressure [18]. Such transition can be observed also for the bulk solids, but under appreciably larger pressure.

The far-reaching hypothesis [19,20] that nanocrystallites of carbon may adopt a truncated icosahedral structure (fullerenes), which is distinctly different from the lattice structure of sp^2 (graphite) or sp^3 (diamond) carbon, was verified experimentally almost two decades later, only [21,22]. To explain the structure of fullerenes, twelve 5-membered rings were proposed to be disposed within the hexagonal network (honeycomb lattice) of graphite. Another kind of related structures, consisting of units of nested fullerenes, i.e. fullerenes with a few shells each, was recently proposed [23,24] and NT with hemispherical fullerene cap have been observed as well [25]. Still more complicated structures, generically known as Schwartzites, can be obtained through the introduction of 7-membered rings imposing negative Gaussian curvature and 5-membered rings (positive Gaussian curvature) into the hexagonal network of graphite [26,27]. This leads to a whole new brand of possible solids, only a few of the topological building blocks of such solids, e.g. helical NTs [28], have been observed so far.

The above work has alluded to a new strategy for the synthesis of nanophases of 2-D (two dimensional) layered compounds with a radically different structure from the bulk material, which is the subject of the present chapter. Subsec.1.2 discusses structural aspects and some unique characteristics of layered compounds, in brief. Sec.2 is dedicated to inorganic fullerenes and NTs from layered compounds. The synthesis of these materials are discussed in Subsec.2.1, the limited knowledge of their global and molecular structure is reserved for Subsec.2.2, where part a is devoted to the experimental work and part b to theoretical aspects of the concept. The conclusions are reserved for alluding various difficulties in the investigation of IF and for identification of possible routes for future progress.

1.2. Layered materials

There are many solids which adopt a highly anisotropic structure (for a review of the structure and properties of various families of compounds with a 2-D structure one may consider Refs. 29-31). The atoms in each layer of a 2-D solid are chemically bonded, usually through a tight covalent bond, while the various layers are stacked together with the help of a weak van der Waals (vdW) force. In energy terms the chemical bonds within the layer ($\perp c$) are about two orders of magnitude stronger than the vdW forces between the layers ($\parallel c$). This leads to a strong anisotropy in the properties of 2-D compounds. A schematic illustration of the crystal structure of MoS_2, which is an archetype of a large group of metal-dichalcogenide 2-D solids, is shown in Fig. 1.

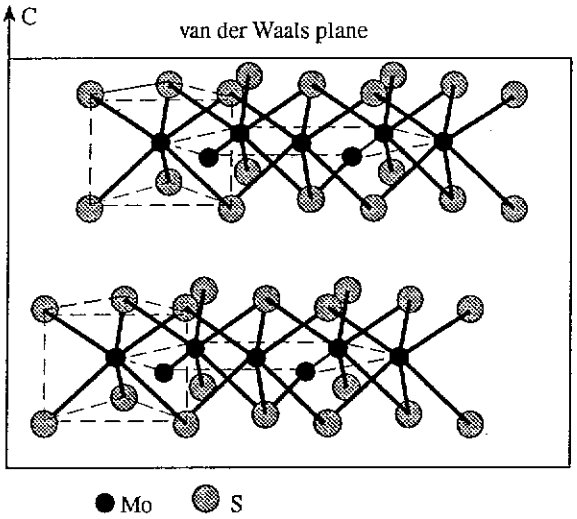

Fig. 1. Schematic drawing of the crystal structure of 2H-MoS_2.

Here each layer consists of three atomic planes with the metal plane sandwiched between two outside sulphur planes. Strong covalent Mo-S bonds operate between the atoms of each layer. Most compounds belonging to this category exhibit polytypism. Thus MoS_2 can be found, in addition to its stable 2H (hexagonal unit cell with two MoS_2 layers as a repeat unit), also in the 3R polytype

(rhombohedral unit cell with three MoS_2 layers as a repeat unit), which is stable at elevated temperatures, only. A schematic drawing of the two polytypes is shown in Fig. 2.

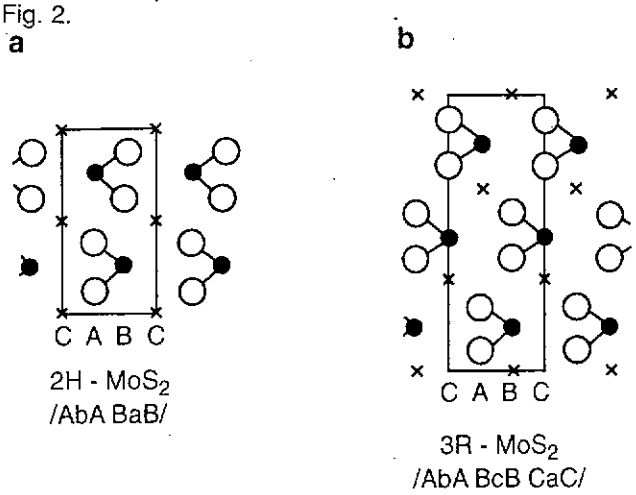

2H - MoS_2
/AbA BaB/

3R - MoS_2
/AbA BcB CaC/

Fig. 2. Schematic drawing of the two polytypes of MoS_2: a. 2H -hexagonal unit cell with two layers as a repeat unit; and b. 3R -rhombohedral unit cell with three layers as a repeat unit.

The large anisotropy of 2-D solids has important ramifications on the chemical reactivity of the two perpendicular faces of such compounds. The sulphur atoms on the (0001) face (designated also vdW or $\perp$c face) of MoS_2 are fully bonded and hence they are chemically very inert. This property makes this surface particularly suitable for solid lubrication. On the contrary, highly reactive dangling bonds occur on the IIc (11-20) face of this material, which lends itself for catalytic applications [32].

To understand the driving force for the formation of IF, NTs and Schwartzites from layered compounds, it is necessary to consider the balance between the following few energy terms: the cohesive energy of the material (E_C) which is proportional to the volume of the material; the surface energy, which can be divided into two components: $E_{S//}$ - parallel to the c- axis, and $E_{S\perp}$- perpendicular to this axis; and finally, the elastic energy due to bending of the layers (E_b). In a macroscopic crystal the surface to volume ratio is small and hence the total energy is dominated by E_C. If now the crystal is divided some 10^7 times, the share of the surface energy in the global energy balance of the nanoparticle, is large. The energy of the free IIc surface becomes predominant to such an extent that it pays the cluster to bend and close on itself. Although the bending introduces a certain strain (E_b>0) into the crystal, this excess energy is more than compensated by elimination of the dangling bonds (the $E_{S//}$ term). Thus, the main driving force for the generation of closed polyhedra (IF), NTs and Schwartzites from layered compounds can be ascribed to the elimination of dangling bonds from the nanocrystallites. Practically, it is not easy to produce IF through the above procedure, which involves massive cleavage of existing bonds. Rather, amorphous precursors are a better starting point for IF formation because they lack the long range order which stabilizes the bulk crystal. Still a better synthetic route for IF is through gas phase reaction. In this case, each unit (nanoparticle) is free to interact

with the carrier gas only, and hence adopts a topology of minimum energy, irrespective of the rest of the nanoparticles.

The interest in quantum size effects and hence in the synthesis of nanophase-materials of layered compounds, is a decade old. In the next section a few of the most typical and unique methods for the synthesis of nanomaterials of layered compounds will be briefly discussed. Their relevance to the synthesis of IF will be emphasized.

1.3. Preparation and structure of nanocrystallites and colloids of layered materials.

The preparation and characterization of colloidal solutions of layered materials have been reported before. Nozik and Peterson [33] presented an excellent review of much of the earlier work. This review evoked also the controversy over the size quantization phenomenon in these kind of materials (*vide infra*). The controversy stems from the fact, that in the absence of a mechanism to stop the growth of the nuclei, size-distribution of nanocrystallites in this group of materials is not easily controlled. Moreover, the reactivity of the dangling bonds on the IIc face of the crystallite leads to an ambiguity with respect to the surface termination of the nanocrystallites. In the absence of a unique way to control the reactive dangling bonds on the ||c face of the nanocrystallites, various reactions can take place on this surface. For example, reaction with oxygen or water will lead to a partial oxidation of the atoms along the ||c face. An intriguing observation in boron-nitride nanoparticles, whereby hemispherical fullerene-like structures were obtained at the ||c edges as a result of the recombination between nearby layers, was reported [34]. IF offer a unique opportunity to get around these problems, since they do not dispose any dangling bonds at their surface, and much better size-control can be possibly attained.

Colloid solutions of a few layered compounds, like PbI_2 [35] and BiI_3 [36] have been prepared through the conventional route of mixing dilute solutions of the salts containing the two ions. This method can not be easily adopted for the preparation of IF because the interaction of the solvent with the dangling bonds on the IIc edges relaxes the excess surface energy - $E_{S//}$ and consequently the stimulus for bending and closure disappears. Furthermore, the reaction is carried-out near room-temperature whence no means to overcome the energy barrier due to strain of the bending layers, could be provided. However, this method is ideally suited for the preparation of the nanosize IF precursors. Subsequently, the precursors could be isolated and heated to yield copious amounts of IF. A method which is unique to layered compounds is the intercalation/exfoliation technique [37], in which Li is first intercalated into the crystal and subsequently the sample is dumped into water where it disintegrates into nanoparticles, some made of a single layer only. Another useful technique for the preparation of colloids and nanoparticles of layered compounds is by sonification of MoS_2 and WS_2 suspended powders in water under hydrogen atmosphere [38]. The latter two methods could be useful for the production of IF because they are violent and the interaction of the dangling bonds with the solvent is not complete. However, both techniques use the precrystallized material, which is not amenable to adopt a new crystalline structure, easily.

A new method for the preparation of nanocrystalline phases of layered materials [39], consists of doping of a sol-gel glass by a cation like Pb, followed by annealing of the glass in the gas atmosphere of iodine. The resultant composite phase, contains a matrix of the oxide (SiO_2) and PbI_2 nanocrystallites embedded in it. The size distribution of the nanocrystallites, is expected to reflect the size distribution of the pores in the host material.

2. Inorganic fullerenes

2.1. The synthesis of inorganic fullerenes

Materials with layered structure can not be obtained through a martensitic transformation of isotropic (3-D) materials. A crystallographic transformation which involves minute rearrangements of the lattice atoms can not bring about a transformation from an isotropic to a 2-D (aniosotropic) compound. This implies that major rearrangements of the lattice occur on the phase boundary of 2-D layered compounds. This situation is particularly favorable for the nucleation of nanocrystallites, and hence to the formation of IF.

Obviously the synthetic routes that lead to the production of colloid solutions of 2-D materials [33,35] are not suitable here, because the saturation of the dangling bonds at the edges of the platelet by solvent molecules is prohibitive for the production of IF. Also, the synthesis of IF is not favorable at low temperatures, in general. The elastic strain involved in bending of the film means that, investment of energy in early stages of the process, is a must. This energy can be provided also from various sources, e.g. irradiation of the sample with electron beam[24], or high energy particle beam (ion beam) [40]. Such routes are unlikely to become mainstream methods for the synthesis of IF nanophases, due mainly to the low yields and prohibitive costs involved. However, they play an instructive role in the elucidation of the growth mechanism of fullerenes.

One of the most widely used method to produce nanophases, is through aerosol reactions [41]. According to this synthetic route an aerosol is obtained by mixing a carrier gas with the precursor (which can be in a form of gas or solution). The aerosol goes first through an oven where cracking of the precursor takes place and then expands through a narrow nozzle, which leads to fast cooling and clustering. Variations of many kinds on this process are known.

In order to locate the window of conditions most appropriate for the synthesis of IF, one must consider the phase diagram of the layered structure compound from which it is derived. A demonstration of this idea is presented in the phase diagram of the W-S system, illustrated in Fig. 3. Supposedly, the IF phase can be obtained on the phase boundary between the amorphous WS_3 precursor and the crystalline 2H-WS_2 phase. The loss of sulphur triggers the nucleation of WS_2 nanocrystallites. If the rate of growth is slow enough the isolated nano-nuclei can not grow into large crystallites at once, and hence they transform first into fullerene-like nanoparticles. Once these particles grow beyond, say 200 nm, they become unstable and 2H-WS_2 platelets are formed.

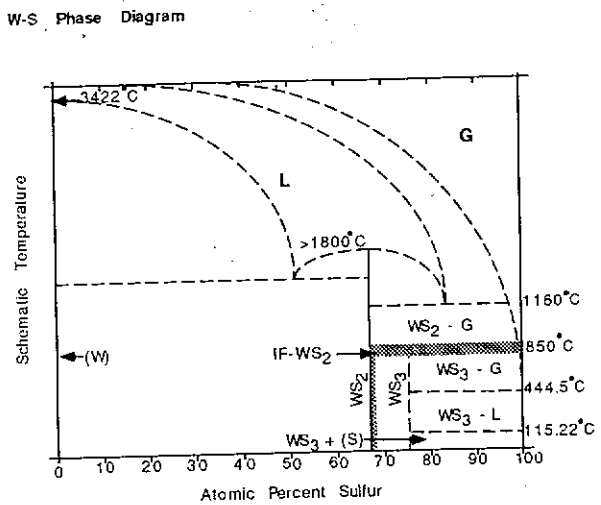

Fig. 3. Phase diagram of W-S. The existence zone for the IF-WS_2 phase is shaded.

IF phases were found to be stable at elevated temperatures for at least a few hours, which indicates that this phase is not a pathological result of the synthetic process. But since the phase boundary between amorphous WS_3 and crystalline 2H-WS_2 extends down to room temperature, one would expect to see spontaneous IF formation from WS_3 precursors even at ambient conditions. Indeed, WS_3 samples which were left at room temperature and inspected from time to time, started to develop "hot spots" after about one year. The "hot spots" started to slowly crystallize, while new "hot spots" appeared throughout the time. After two years a few of them exhibited developed IF morphology. This process went on and many new IF were formed after 3 years from the time they were first put in the drawer. IF which were prepared at elevated temperatures and kept in the drawer since for a long period of time, did not show any evolution after a few years time and are therefore considered to be stable at room temperature, "indefinitely".

Although there is some disagreement concerning the occurrence of an amorphous MoS_3 (a-MoS_3) phase, a few reports indicated that this is the dominant phase in the Mo-S phase diagram at low temperatures and excess sulfur regime [42]. On elevating the reaction temperature, the 2H-MoS_2 polytype predominates. This situation, which is represented by reactions 5 and 6 on the ternary phase diagram (Fig. 4), is favorable for the growth of IF-MoS_2, because by losing sulphur, the a-MoS_3 phase is expected to slowly transform into nanocrystallites of MoS_2 and spontaneously collapse into IFs [43c]. This is believed to be the main growth mechanism of IF in the solid (MoO_3)-gas (H_2S) reaction described below.

Three kinds of synthetic routes have been successfully pursued for the "large scale" synthesis of IF in our laboratory. They are based on gas-solid and gas phase reactions. In the early days of this work, thin film (typically 10 nm) of metal or metal oxides were deposited on a quartz substrate and fired in a reducing atmosphere containing H_2S (S) [43].

While this method was useful for the production of a plethora of IF structures and nanotubes from MX_2 compounds (M=Mo,W;X=S,Se), it was unlikely to yield a large quantity of a single phase IF and particularly not one with a narrow size-distribution. Utilizing the analogy to carbon fullerenes [44], it was suggested that the ideal growth conditions for the IF phase could be provided through a gas phase reaction. In this case, each nanocluster is isolated in the reaction chamber and the only means for it to release its extra energy is through collisions with the noble carrier gas (He in most experiments). To produce IF-MoS_2 through this route, a careful consideration and a detailed knowledge of the phase equilibria in the reaction chamber was necessary. However, the choice of source materials for a gas phase reaction is fairly extensive. For example, preparation of MoS_2 powders and films by the gas phase reaction between $MoCl_X$ (X=3-5) and H_2S [45] or MoF_6 and H_2S [42] has been demonstrated. Alternatively, pulsed laser evaporation [46], metal organic chemical vapor deposition [47], and so forth, can be used to form IF from the gas phase. In order to take advantage of the sublimation of MoO_{3-x} at relatively low temperatures (>650°C), a reactor was built that allowed for a gas phase reaction between a stream of gaseous molybdenum suboxide and H_2S [48]. This reactor was used to prepare, reproducibly, a few milligrams of an almost pure IF phase in each run.

In order to form MoS_2 from H_2S and MoO_3 in a reducing atmosphere at elevated temperatures, the Mo-S-O ternary phase diagram should be considered [49] (see schematic ternary phase diagram in Fig. 4).

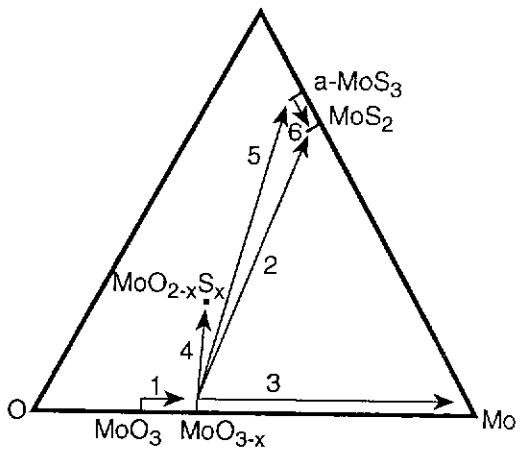

Fig. 4. Ternary phase diagram for Mo-S-O. The numbered arrows represent the various reactions described in the text (Eqs.1-6).

The following series of reactions are relevant for the synthesis of MoS_2:

$$MoO_3(s) + XH_2(g) \rightarrow MoO_{3-X}(g) + XH_2O(g) \quad (1)$$

$$MoO_{3-X}(g) + (1-X)H_2(g) + 2H_2S(g) \rightarrow MoS_2(s) + (3-X)H_2O(g) \quad (2)$$

$$MoO_3(s) + 3H_2(g) \rightarrow Mo(s) + 3H_2O(g) \quad (3)$$

$$MoO_{3-X}(g) + (1-X)H_2(g) + XH_2S(g) \rightarrow MoO_{2-X}S_X(s) + H_2O(g) \quad (4)$$

$$MoO_{3-X}(g) + 3H_2S(g) \rightarrow MoS_3(s) + (3-X)H_2O(g) + XH_2(g) \quad (5)$$

$$MoS_3(s) \rightarrow MoS_2(s) + S(g) \quad (6)$$

Nonstoichiometry commonly occurs in metaloxides, including the molybdenum compounds. One may also take advantage of the fact that some of the substoichiometric oxides are very volatile and sublime at temperatures as low as 650°C (reaction 1). However, if the reducing atmosphere is too strong, metallic molybdenum, which has an exceedingly low vapor pressure at these temperatures (reaction 3), occurs. On the other hand if the reducing atmosphere in the reactor is not sufficiently strong, oxi-sulfides of molybdenum with an orthorhombic structure are collected on the substrate (for example, reaction 4). Careful control of the reducing atmosphere in the reaction chamber is a prerequisite for the successful production of the elusive IF phase through reaction 2.

A schematic illustration of the reactor used to prepare copious amounts of IF-MoS_2 is shown in Fig. 5. In one design (a) the fluxes of the two gases were not separated. This reactor yielded copious amounts of IF of a small size (<6 nm) and one or two layers thick. Single layer NTs as long as 15 μm and negatively curved IF (Schwartzites) were obtained in this reactor as well. Macroscopic quantities of multiple shell IF (onions) of a relatively narrow size distribution, were obtained in a reactor of kind (b). The gas fluxes were separated in this reactor, using an additional tube filled with MoO_3 powder. The exit of this tube was turned 90° with respect to the main gas stream and the size and shape of the nozzle was carefully designed.

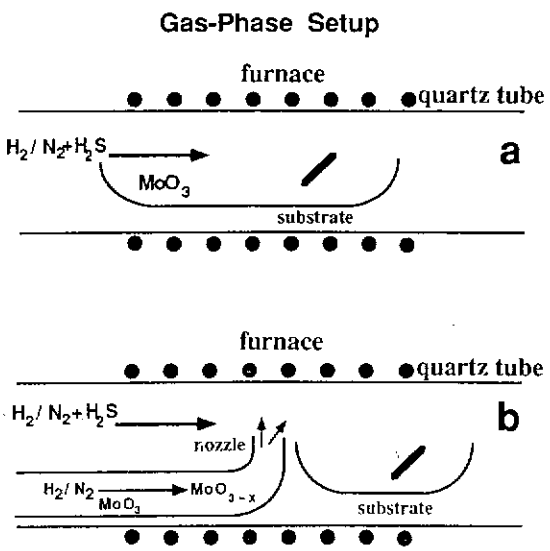

Fig. 5. Schematics of the two gas-phase reactors used to synthesize pure phase of IF-MoS_2 and NTs. a. reactor for the synthesis of single and double layer IF of a diameter <10nm (taken from Ref.48b); b. reactor used in Ref.48a to obtain large quantities of a pure IF-MoS_2 phases of various sizes.

To ensure the appropriate reducing atmosphere in each of the gas streams, two separate sources of forming gas (5%H_2/95%N_2 mixture) were necessary. The flow of the various gases was automatically controlled. Any small change in the flow regime adversely influenced the reaction products. A turbulent flow regime was maintained. This flow regime was responsible for the thorough mixing of the reacting oxide and H_2S gases which was found to yield the best and most reproducible results. In order to produce this turbulent regime, the collecting quartz substrate was put behind a high wall of the boat. The quartz slides with the products were used as such for the x-ray diffraction (XRD), optical and photoelectron measurements, or the products were transferred onto amile acetate coated Cu grids for inspection in a TEM.

Another synthetic route, which yielded "gram" quantities of IF-WS_2 with diameters ranging from 50 to 100 nm, was through firing of a finely divided powder of WO_3 under reducing atmosphere and H_2S gas stream [50]. It appears that in this case the size of the WO_3 grains, determined the size of the IF. The oxygen-sulphur exchange was followed in this case, which provided important mechanistic details of the conversion reaction. This kind of synthesis, which will not be further elaborated here, can yield IF with a narrow size distribution by utilizing an oxide powder with a uniform nanograin-size. Preferably, each nanograin must be grown in isolation, e.g. through a floating bad reactor. Also, IFs of a diameter smaller than say 5 nm, can not be easily obtained in this way.

2.2. Structural characterization of IF and NTs

2.2.a. Experiments

A series of TEM images from the various reaction products, which were obtained at different temperatures, is shown in Fig. 6. For temperatures up to 800°C an amorphous phase was obtained (Fig. 6a) which yielded a broad peak in XRD and a fuzzy electron diffraction pattern. Growth at 820°C produced IFs ~ 20 nm in (external) diameter (Fig. 6b). The average size of the IFs increased with increasing reaction temperature. A typical example obtained at 840°C is shown in Fig. 6c. Here the average external diameter is ~ 40 nm. When the reaction was allowed to proceed for 2 hours instead of 1 hour, there was no noticeable change in the IF size distribution. This result suggests that the sizes and morphologies of the IF are determined during growth in the gas phase. It further alludes to the possibility that the products of the gas phase reaction were obtained under quasi-equilibrium conditions, so that a theoretical analysis using equilibrium mechanics is warranted (see below). At a growth temperature of 900°C, the external diameter of the IFs was 100 nm and the wall thickness was ~ 20 nm (Fig. 6d). Platelets of 100 to 300 nm size and above, belonging to the 2H-MoS_2 polytype, start to appear at this temperature. If the temperature of the reactor is further increased, the fraction of the 2H-MoS_2 predominates and becomes the sole phase at 950°C. Higher annealing temperatures yielded even larger crystallites of the same phase. The IFs represented the most prevalent phase in the film only under a specific turbulent flow regime. They were visible only sporadically under laminar flow regime even at temperatures (840°C) where IFs predominate under turbulent flow regime (Fig. 6e). A high-resolution image of two IFs obtained at 840°C is shown in Fig. 6f.

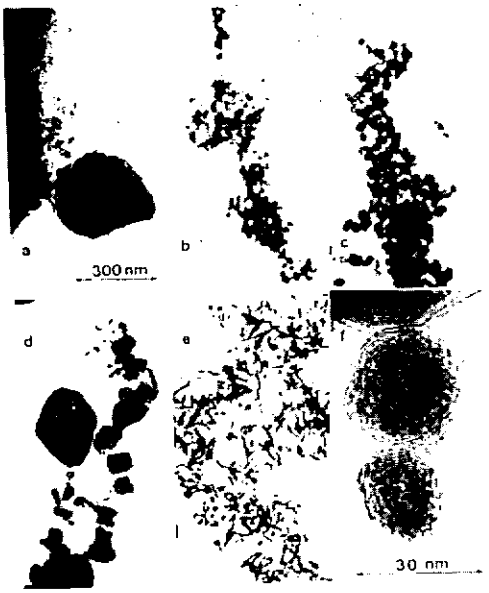

Fig. 6. A series of TEM images showing the structure of IF-MoS_2. a. Amorphous phase produced at 800°C; b. IF of 20 nm average size obtained at 820°C; c. IF of 40 nm average size obtained at 840°C; d. Mixed IF (100 nm average size) and platelets (100 to 300 nm) obtained at 900°C; e. 2H-MoS_2 phase prepared at 840°C under laminar flow regime; f. High-magnification image of two typical IF obtained at 840°C. Distance between each two fringes is c/2=0.62nm. The fluxes of the various gases in the reactor are: H_2S, 1.5cm^3/min; H_2(5%)/N_2(95%), 90cm^3/min in main tube, and 30cm^3/min in the inner tube (see Fig. 5b). The copper grids for the TEM experiments were covered with amyl acetate film in order to close the gap between the Cu filaments. A 5-nm amorphous carbon film was deposited on top to render the insulating film conductive.

In contrast to carbon fullerenes, where carbon rings with less than 5 atoms are unlikely, IF-MoS_2 can afford stable 3- and 4-membered rings. Evidence for the existence of such point defects in IF are abundant [43b].

The spacing between two adjacent layers in CF (c/2) and NTs was found to be somewhat larger than that of bulk graphite [51]. The lattice expansion was ascribed to strain relief in the folded structure. A similar mechanism for strain relief was expected to operate in the case of IFs as well. A series of XRD spectra for the various films prepared on quartz substrates is shown in Fig. 7. The (0002) peak position in the XRD pattern depended not only on temperature but also on the flow regime, as expected from the TEM results. The XRD pattern for the film prepared in the turbulent flow regime at temperatures between 800° to 900°C corresponded to the IF phase seen in TEM. The sample prepared at 840°C showed an average expansion of 2% along the c axis (Fig. 7 curve a) compared with the 2H phase (vertical line). The average size of the crystallites was calculated from the Debye-Scherrer formula to be 40 nm (see also Fig. 6c).

Upon increasing the temperature to 900°C (Fig. 7 curve b), the intensity of the peak increased and its position was closer to the 2H phase peak (see also Fig. 6e). The average size of the crystallites was 100 nm at this temperature, which suggests a reduced strain for the larger IF. The XRD spectrum of the specimen obtained within the laminar flow regime (Fig. 7 curve c) at 840°C (see also Fig. 6e) corresponded to the 2H bulk phase. The XRD spectra of the samples which were heated to T≥950°C corresponded to the bulk 2H phase, independent of the flow regime. The XRD results were consistent with the TEM observations and confirmed the growth of the IF phase. Both the TEM and XRD results confirmed the importance of the turbulent flow regime for the production of the IF phase. The increased van

der Waals gap (c/2) of the IF suggests an easier intercalation of small alkali ions into the IF compared with the bulk 2H polytype.

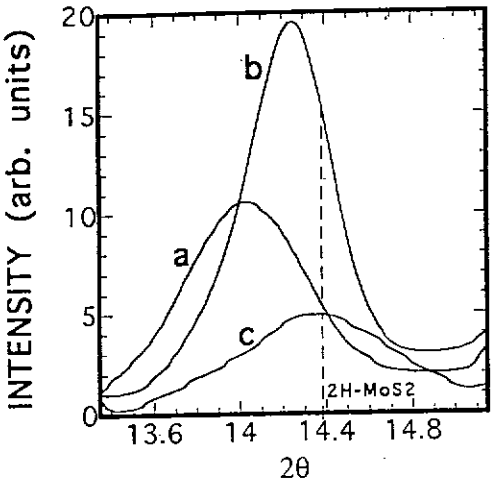

Fig. 7. Powder XRD spectrum taken from the phases obtained during the growth of MoS_2 at: a. 840°C; b. 900°C; and c. 840°C under laminar flow conditions.

When the nozzle of the exit gas mixture containing MoO_{3-x} was made very narrow, substantial amounts of NTs were obtained (Fig. 8).

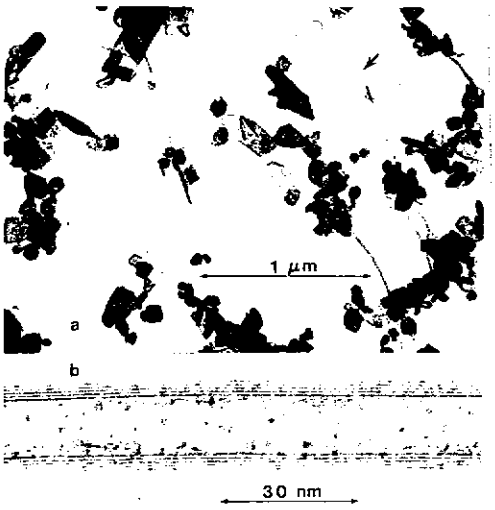

Fig. 8. a. Assortment of NTs obtained by the gas-phase reaction of MoO_{3-x} and H_2S in a reducing atmosphere at 850°C; b. High-magnification image of the arrowed tube. Distance between each two fringes is c/2=0.62nm. Taken from Ref.48b.

The slender NTs, which were obtained in this way, had diameters ranging from 10 to 20 nm. They were a few μm long and very uniform in shape (Fig. 8b). In fact, many of the NTs were cut during the transfer process onto the Cu grid. The NTs were mixed with a separate phase consisting of 2H-MoS_2 platelets. This process

allows a production of copious amounts of NTs, although still not as reproducible as in the case of IF. In the absence of any metallic catalyst, which is often used in the synthesis of carbon NTs, it is possible that the prevailing mechanism for the formation of the NTs is the open-ended growth [52]. This model describes the growth mechanism as an addition of Mo and S atoms to the edge of the NT, where the presence of dangling bonds induces large sticking coefficients for the incoming Mo and S atoms. This is not the only possible growth mechanism for MoS_2 NTs in this reactor, however. An alternative explanation is that a single MoS_2 layer (the analog of a graphene sheet in carbon), comes out of the reactor and folds on itself to form the first layer of the NT. This first layer serves as a template, whereupon multiple MoS_2 layers are added during the growth of the multiple shell NT. In a few cases, while using the single compartment reactor (Fig. 5a), needle-like MoO_3 nanoparticles which converted into single layer MoS_2 NTs, were found on the surface of the collector [50]. It is likely that in this case the needle-like MoO_3 nanoparticles were first deposited on the quartz collector and were gradually transformed into a single layer MoS_2 NTs.

Fig. 9 shows a typical structure exhibiting a negative curvature (arrowed) [53]. This NT, which was obtained with the single compartment gas-phase reactor (Fig. 5a), is similar to the branched structures reported for carbon, recently [54]. The mechanism of branching, which yields structures with negative curvature, is not clear at this point. No evidence for a metal (Mo) assisted catalytic growth mechanism exists in this case. It is believed that in order to obtain negative curvature with 90° angle between the two branches, an array of four 8-membered rings are disposed along the perimeter of the branched tube [53].

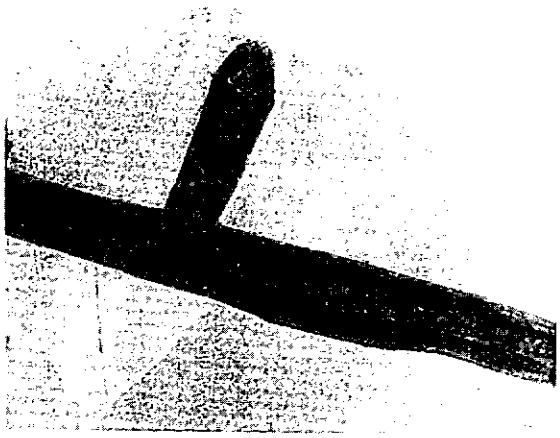

Fig. 9. TEM image of a typical structure exhibiting negative curvature, obtained by gas-phase synthesis with a single compartment reactor. Distance between the two fringes is c/2=0.62nm.

Wrapped hexagonal sheets can form non-helical or helical cylinders (NT). For the latter ones the helicity angle could be estimated from diffraction patterns. From the chirality point of view, they might be either right- or left-handed. It is well known that a helical object viewed in a direction perpendicular to its axis, exhibits a symmetrical image. When the helix axis is tilted with respect to the direction of view, an asymmetry arises. This phenomenon was earlier applied for the chirality

determination of tobacco mosaic virus [55] and for the confirmation of the helical structure of Pf1 filamentous virus [56].

Two ways for identifying the asymmetry by TEM may be foreseen: observations in high resolution mode, or using the dark-field diffraction contrast in conventional TEM. Several examples confirming that such an asymmetry has been actually observed in carbon NT, by high resolution TEM (see, for example, Fig. 4 in Ref. 57a and Fig. 10 in Ref. 57b), but not recognized, are known. The second way is described in more detail below [58].

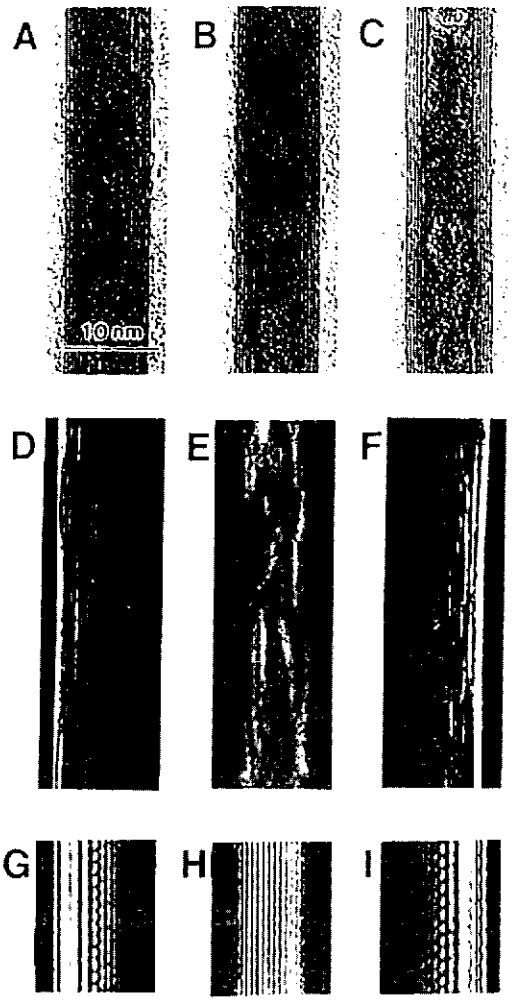

When a chiral NT is tilted with respect to the incident electron beam, different diffraction conditions are realized for the two sides of the NT. In this case the atomic rows come closer to the exact diffraction position on one side and go out of diffraction conditions on the opposite side.

Hence, the diffraction contrast is asymmetric on the two sides of the NT image, and the best way to visualize this asymmetry is realized in dark-field microscopy. One can observe, by an appropriate selection of the tilt angle and the reflection for dark-field imaging, a huge difference in the diffraction contrast of the two sides of the NT and thus determine its chirality. If one knows the tilt direction, the NT chirality can be unambiguously determined from the dark-field contrast asymmetry. Fig. 10 combines the experimental bright- and dark-field images as well as computer simulations for a right handed NT.

Fig. 10. Experimental (a-f) and simulated (g-i) images of a right-handed mono-helical nanotube whose tilt positions correspond to the scheme shown in fig. 1. One can clearly see the symmetry of lattice fringes of basal planes in bright-field images (a-c) and asymmetry of the dark-field contrast for the tilted positions (d, f).

The bright-field images of basal planes remain the same on both sides of the NT for all tilting positions (Fig. 10 A-C). The dark-field micrographs (Fig. 10 D-F), taken from reflections of {10.0} type, demonstrate an asymmetry of the image contrast for the tilted NT. These images correspond very well to the computer simulations (Fig. 10 G-I) made by the Fourier filtering technique. Thus, The dark-field technique presented here allows to determine the chirality of mono-helical nanotubes.

2.2.b. Theoretical considerations

Recent experimental and theoretical work [24,57,58] suggest that carbon-based nested fullerenes (also known as onions, multilayered or Russian doll fullerenes) are more stable than single shell fullerenes when the number of carbon atoms exceeds a critical size N_c ($N_c>10^3$). The energy of a nested fullerene has three main components: the curvature or bending elastic energy, the defect (dislocation) energy and the surface energy. To get information on the possible equilibrium structures, a continuum elastic theory was developed [48b,59], which takes into account these three terms. This theory was used to demonstrate that either dislocations or grain boundaries (an ordered array of dislocations) are an intrinsic component of thick walled, nested fullerenes. Experimental evidence, consistent with this picture, which shows that nested fullerenes with small thickness show a spherosymmetric shape while thick, nested fullerenes show either faceted or non-faceted shapes associated with grain boundary or dislocation relaxed structures, was presented.

The importance of dislocations can be understood by considering a 2-shell, spherical graphitic fullerene where geometry dictates that the outer shell contains more atoms than the inner shell. These two shells cannot pack together perfectly like the (0002) planes in graphite. While locally the layer packing may be similar to graphite, the regions of good lattice match must be separated by discommensurations or, equivalently, dislocations. Hence any discussion of the energetics must include these geometrically induced defects.

For a sphere of radius $R=1/\kappa$ (R is the distance from the center to the middle of the spherical shell), the bending energy is: $E_b=\chi d^3\kappa^2/12$, where $\chi = 2k + \bar{k}$ (k and $\bar{k}$ are bending mudulii). This expression assumes that the whole thin film bends coherently. However, if the atomic planes can slip without resistance, the elastic energy is relaxed to $E_r=\chi dc^2\kappa^2/12$, where c =c/2 is the spacing between atomic layers. This energy is simply the energy W_u to independently bend d/c layers of a thickness c.

When the crystal planes in a thin film slip relative to each other, the crystal structure is disrupted. When this slippage is localized in the form of dislocations, rather than continuously distributed across the shell, the crystal structure is disrupted less and this slippage is energetically less costly. Taking into account the dislocation energy, it can be shown that for $\kappa<\kappa_c$ and thickness (of IF wall) to

radius-h/r<<1, the IF assumes a uniform bending. However, for $\kappa > \kappa_C$ the elastic energy is reduced upon bending by forming an array of dislocations of a constant density. For a fixed curvature one may think of a critical thickness, below which the layers bend without any dislocations and above which dislocations pope-in. The theory shows that for thin nested fullerenes the value of critical curvature is rather high, and one might expect them to grow relatively dislocation free. Dislocations tend to organize themselves into grain boundaries and theory [48b,59] predicts that thin, nested fullerenes would tend to be grain boundary free and show spherically symmetric morphologies. A surface energy term must be included as well in this calculation. Adding this term one finds that for the uniformly bended IF (and also CF), the most stable cluster should have h/r ratio of ~0.1-0.2, which is often the case in the gas-phase synthesis (Fig. 11).

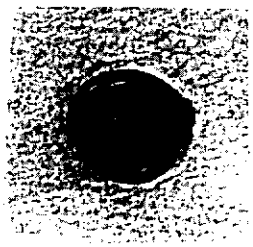

Fig. 11. TEM image of a typical IF-MoS_2 with small diameter (6nm) and two layers, obtained by gas-phase synthesis with a single compartment reactor. Distance between the two layers (c/2) is 0.62 nm.

Furthermore, the most stable dislocated IF structure is found to be the one with grain boundaries, i.e. faceted IF.

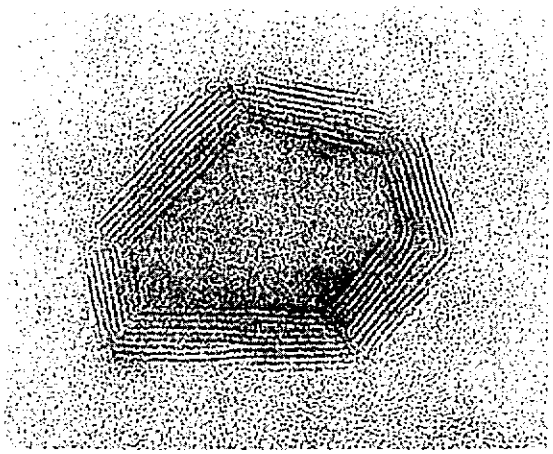

Indeed, in a number of cases highly faceted IF were observed as shown in Fig. 12. From the mechanistic and theoretical point of view, it would be very instructive to follow the evolution of a single IF by repetitive inspection/annealing cycles, which is unfortunately a very difficult task at this point.

Fig. 12. TEM observation of a faceted IF-WS_2 structure. Distance between the two fringes is c/2=0.62nm.

Since the theory is macroscopic in nature it can not elaborate on the nature of dislocations that occur in the fullerene structure, which is a major obstacle for further progress in understanding the structure of IF. Furthermore, lattice expansion in c direction was not considered, although doubtlessly this is a major relaxation mode for the strained IF structures. This point is well taken and will be addressed in future analysis.

3. Concluding remarks

The present work shows that the scope of fullerene-like materials is broader than previously thought. Nanocrystallites of many layered compounds can be

anticipated to follow the same instability and adopt a hollow-cage structure. The main issue here is to attempt to determine the type of polygons which are involved in the curvature of the atomic planes. Since the structure of most layered compounds is appreciably more complicated than that of graphite, the topology of the polygons is likely to be more complicated. Another issue is the study of the existence zone of the IF phase in the phase diagrams of layered compounds. In the case of WS_2 the existence zone for the IF phase is known with quite a good confidence. The properties of the IF phase of layered compounds can not be studied unless sufficient quantities of the material exists. It is hoped that the development of more sophisticated methods for the synthesis and isolation of the material will enable the systematic study of these materials.

Acknowledgment: I am indebted to many of my colleagues and students who contributed to this work: Dr. L. Margulis, Dr. G. Hodes, Prof. S.A. Safran, Y. Feldman, G. Frey, M. Homyonfer, and Dr. P. Dluzewski of the Weizmann Institute, Dr. E. Wasserman of E.I. du-Pont de Nemours, Prof. D.J. Srolovitz of Michigan University (Michael fellow of the Weizmann Institute in 1994), and Dr. J.A. Hutchison of Oxford University. This work has been supported by grants from the US-Israel binational foundation; Israeli Ministries of Energy and Infrastrucutre and Science and Arts; the H. Levine and Edith reich foundations of the Weizmann Institute.

References

1. A.L. Mackay, *Acta Cryst.* **15**, 916 (1962).
2. J.F. Sadoc, J. Dixmier, and A. Guinier, *J. Non-crystalline Sol.* **12**, 76 (1973).
3. C.L. Briant and J.J. Burton, *Phys. Stat. Sol. (b)* **85**, 393 (1978).
4. M.R. Hoare, *Ann. N.Y. Acad. Sci.* **279**, 186 (1976).
5. F.C. Frank, *Proc. Royal Soc. London Ser. A* **215**, 43 (1952).
6. R.R. Winters and W.S. Hammack, *Science* **260**, 202 (1993).
7. S. Ino and S. Ogawa, *J. Phys. Soc. Jpn.* **22**, 1365 (1967).
8. P.P. Edwards, *Proc. Mater. Res. Soc. Symp. Chem. Processes Inorg. Mater.*, Eds: P.P. Persans, J.S. Bradley, R.R. Chianelli, G. Schmid **272**, 311 (1992).
9. J. Farges, M.F. de Feraudy, B. Raoult, and G. Torchet, *NATO ASI Ser., Ser. B: Physics*, Eds. P. Jena, B.K. Rao, and S.N. Khanna **158**, 15 (1986).
10. T.P. Martin, T. Bergmann, H. Göhlich and T. Lange, *Chem. Phys. Lett.* **176**, 343 (1991).
11. O. Echt, K. Sattler, and E. Recknagel, *Phys. Rev. Lett.* **47**, 1121 (1981).
12. B. Raoult, J. Farges, M.F. De Feraudy, and G. Torchet, *Z. Physik D* **12**, 85 (1989).
13. C.L. Cleveland and U. Landman, *J. Chem. Phys.* **94**, 7376 (1991).
14. S. Yatsuya, R. Uyeda, and Y. Fukano, *Jpn. J. Appl. Phys.* **11**, 408 (1972).
15. J.F. Sadoc and R. Mosseri, *Phil. Mag. B* **45**, 467(1982).
16. D.R. Nelson, *Phys. Rev. B* **28**, 5515 (1983).
17. S. Iijima, *Jap. J. Appl. Phys.* **26**, 357 (1987) and the following paper.
18. S.H. Tolbert and A.P. Alivisatos, *Science* **265**, 373 (1994).
19. D.E.H. Jones, *New Scientist* **245**, 3 Nov. (1966).
20. E. Osawa, *Kagaku* **25**, 854 (1970).

21. H.W. Kroto, J.R. Heath, S.C. O'Brien, R.F. Curl, and R.E. Smalley, *Nature* **318**, 162 (1985).
22. W. A. Krätschmer, L. D. Lamb, K. Fostiropoulos, D. R. Huffman, *Nature* **347**, 354 (1990).
23. S. Iijima, *J. Cryst. Growth* **50**, 675 (1980).
24. D. Ugarte, *Nature* **359**, 707 (1992); *Eurphys. Lett.* **22**, 45 (1993).
25. S. Iijima, *Nature* **354**, 56 (1991).
26. S. Iijima, T. Ichihashi, and Y. Ando, *Nature* **356**, 776 (1992).
27. a. A.L. Mackay, and H. Terrones, *Nature* **352**, 762 (1991); b. D. Vanderbilt and J. Tersoff, *Phys. Rev. Lett.* **68**, 511 (1992).
28. a. S. Ihara, S. Itoh, and K. Kitakami, *Phys. Rev. B* **48**, 5643 (1993); b. S. Amelinckx, X.B. Zhang, D. Bernaerts, X.F. Zhang, V. Ivanov, and J.B. Nagy, *Science* **265**, 635 (1994).
29. J.A. Wilson and A.D. Yoffe, *Advances in Physics* **18**, 193 (1969).
30. *Preparation and Crystal Growth of Materials with Layered Structures*, Ed. R.M.A. Lieth, D. Reidel Publishing Company, Dordrecht (1977).
31. *Photoelectrochemistry and photovoltaics of layered semicondcutors*, A. Aruchamy Ed., Kluwer Academic Publishers, Dordrecht (1992).
32. a. C.B. Roxlo, M. Daage, A.F. Ruppert, and R.R. Chianelli, *J. Catal.* **100**, 176-184 (1986).
33. M.W. Peterson and A.J. Nozik, in Ref.22, pp. 297-317.
34. L. Boulanger, B. Andriot, M. Cauchetier, and F. Willaime, *Chem. Phys. Lett* **234**, 227 (1995).
35. C.J. Sandroff, D.M. Hwang, and W.M. Chung, *Phys. Rev. B* **33**, 5953 (1986).
36. C.J. Sandroff and W.M. Chung, *J. Colloid Interface Sci.* **115**, 593 (1987).
37. P. Joensen, R.F. Frindt, and S.R. Morrison, *Mater. Res. Bull.* **21**, 457-461 (1988).
38. M. Gutierrez and A. Henglein, *Ultrasonics* **27**, 259 (1989).
39. E. Lifshitz, M. Yassen, L. Bykov, I. Dag, and R. Chaim, *J. Phys. Chem.* **99**, 1245 (1995).
40. 25. L.T. Chadderton, D. Fink, Y. Gamaly, H. Moeckel, L. Wang, H. Omichi, and F. Hosoi, *Nucl. Instr. Methods Phys. Res. B* **91**, 71 (1994).
41. K.A. Littau, P.J. Sjajowski, A.J. Muller, A.R. Kortan, and L.E. Brus, *J. Phys. Chem.* **97**, 1224 (1993).
42. a. E. Furimsky and C.H. Amberg, *Can. J. Chem.* **53**, 3567 (1975); b. W. L. Lee, T. M. Besmann, M. W. Stott, *J. Mater. Res.* **9**, 1474 (1994).
43. a. R. Tenne, L. Margulis, M. Genut, G. Hodes, *Nature* **360**, 444 (1992); b. L. Margulis, G. Salitra, R. Tenne, M. Talianker, *Nature* **365**, 113 (1993); c. M. Hershfinkel et al, *J. Am. Chem. Soc.* **116**, 1914 (1994).
44. Q. L. Zhang et al, *J. Phys. Chem.* **90**, 525 (1986); H. W. Kroto, *Nature* **329**, 529 (1987).
45. H. Arctowski, *Z. Anorg. Allgem. Chem.* **8**, 213 (1895); P. R. Bonneau, R. F. Jarvis Jr., R. B. Kaner, *Nature* **349**, 510 (1991); N. Imanishi, K. Kanamura, Z. Takehara, *J. Electrochem. Soc.* **139**, 2082 (1992).
46. M. S. Donley, N. T. McDevitt, T. W. Hass, P. T. Murray, J. T. Grant, *Thin Solid Films* **168**, 335 (1989).
47. W. K. Hofmann, *J. Mater. Sci.* **23**, 3981 (1988).
48. a. Y. Feldmann, E. Wasserman, D.J. Srolovitz, and R. Tenne, *Science* **267**, 222 (1995); b. D. J. Srolovitz, S. A. Safran, M. Homyonfer, and R. Tenne, *Phys. Rev. Lett.* **74**, 1779 (1995).

49. The role of the hydrogen was considered here as a reducing agent, only. However, hydrogen is known to intercalate into MoO_3 [see, for example, S.P. Mehandru and A.B. Anderson, *J. Am. Chem. Soc.* **110**, 2061 (1988)].
50. Y. Feldman, M. Homyonfer, L. margulis, J.A, Hutchison, H. Cohen, G. Hodes, and R. Tenne, to be published.
51. a. Y. Saito, T. Yoshikawa, S. Bandow, M. Tomita, *Phys. Rev. B*, **48**, 1907 (1993); b. Y. Yosida, *Appl. Phys. Lett.* **64**, 3048 (1994); c. M. Li and J. M. Cowley, *Ultramicroscopy* **53**, 333 (1994).
52. S. Iijima, P.M. Ajayan, and T. Ichihashi, *Phys. Rev. Lett.* **69**, 3100 (1992).
53. M. Homyonfer, L. Margulis, and R. Tenne, to be published.
54. D. Zhou and S. Seraphin, *Chem. Phys. Lett.* **238**, 286 (1995).
55. J.T. Finch, *J. Mol. Biology* **66**, 291 (1972).
56. C.W. Gray, G.G. Kneale, K.R. Leonard, H. Siegrist, D.A. Marvin, *Virology* **116**, 40 (1982).
57. L. Margulis , P. Dluzewski, Y. Feldman and R. Tenne, *J. Microscopy*, in press.
58. a. S. Iijima, *MRS Bulletin*, p. 43, November (1994); b. X. F. Zhang, X. B. Zhang, G. Van Tendeloo, S. Amelinckx, M. Op de Beeck, J. Van Landuyt, *J. Cryst. Growth* **130**, 368 (1993).
59. A. Maiti, C. J. Brabec, and J.. Bernholc, *Phys. Rev. Lett.* **70**, 3023 (1993).
60. J. P. Lu and W. Yang, *Rhys. Rev. B* **49**, 11,421 (1994).
61. D. J. Srolovitz, S. A. Safran and R. Tenne, *Phys. Rev. E* **49**, 5260 (1994).